ELSEVIER

Journal of Chromatography A, 760 (1997) 205–218

JOURNAL OF CHROMATOGRAPHY A

Fast molecular mass and size characterization of polysaccharides using asymmetrical flow field-flow fractionation–multiangle light scattering

Bengt Wittgren, Karl-Gustav Wahlund*

Division of Technical Analytical Chemistry, Center for Chemistry and Chemical Engineering, Lund University, P.O. Box 124, S-221 00 Lund, Sweden

Received 31 May 1996; revised 10 September 1996; accepted 12 September 1996

Abstract

Asymmetrical flow field-flow fractionation (asymmetrical flow FFF), connected on-line to multi-angle light scattering detection (MALS) was shown here to be an efficient method for size characterization of pullulan standards and dextrans ranging from 20 000 up to 2 000 000 in molecular mass. The characterization of molecular mass and the molecular mass distribution of these polysaccharides is often complex and may require different methods. Using asymmetrical flow FFF–MALS, information was obtained not only about molecular mass and molecular mass distribution but also about hydrodynamic size as well as radius of gyration and conformation. The analysis time was very short, often below 5 min. It was shown that the pullulan standards have a narrow molecular mass distribution compared to the more polydisperse dextrans. Obtained molecular masses and distributions were in good agreement with data from the manufacturer. The dextrans, especially at high molecular mass, were found to have a more compact structure than the pullulans in both water and 0.1 *M* NaCl.

Keywords: Molecular mass distribution; Molecular mass determination; Field-flow fractionation; Multi-angle light scattering; Polysaccharides; Dextrans; Pullulans

1. Introduction

Field-flow fractionation (FFF) is a separation method suitable for the characterization of macromolecules and particles [1]. The technique was first described in the 1960s [2] and has since experienced considerable instrumental as well as theoretical development. Flow FFF is perhaps the most universal subtechnique in the family of FFF [1]. It has in several publications been shown to be an effective method for the fractionation and characterization of materials in a wide size range, from 1 nm up to 50 μm. For example, flow FFF is useful in the characterization of water-soluble polymers, such as pullulans [3], dextrans [3], polystyrene sulfonate [4], poly(vinyl pyridine) [4] as well as amphiphilic graft co-polymers [5,6]. Flow FFF is an absolute method in the sense that it has the ability to, without any calibration, determine diffusion coefficients and thus hydrodynamic sizes of macromolecules and particles [1]. However, the transformation from diffusion coefficients into the often more desired molecular

*Corresponding author.

PII S0021-9673(96)00777-7

mass is not obvious. Attempts to use Mark-Houwink constants for the conversion of diffusion coefficients into molecular masses have been reported for dextran, pullulan, poly(ethylene oxide) and polystyrene sulfonate [3].

Connecting flow FFF to multi-angle light scattering detection (MALS), may be a successful way to obtain molecular masses and distributions. By the measurements of light scattering at several angles, it is possible to get information also about the radius of gyration. This option together with the hydrodynamic diameter given directly by flow FFF elution times is an additional advantage of the connection. A few studies have been reported, where flow FFF–MALS was employed in the size characterization of polystyrene latex and a dextran [7], polystyrene particles [8], and sulfonated polystyrene standards [9], and the results are very promising. In this report we describe the connection between the asymmetrical variant of flow FFF and MALS. Asymmetrical flow FFF has previously been used in several applications [5,6,10] and has turned out to be a rapid and efficient way of conducting flow FFF.

Polysaccharides are an important group of water-soluble polymers and are used in many different applications in for example food additives and drug formulations. One effect of the increased interest is a growing need for information about the solution properties of the polysaccharides. Knowledge about the molecular mass and molecular mass distribution is essential in order to predict their behavior in processes and products. The traditional method for molecular mass characterization of water-soluble polymers is size-exclusion chromatography (SEC). One limitation using SEC is the possible total exclusion or degradation of large sized macromolecules, which would cause errors in the molecular mass distribution. This might be especially considered when working with the characterization of polysaccharides, e.g. starch, or modified cellulose, whose polydispersity is large and where large-sized aggregates up to several hundred nm may occur. The connection of sedimentation FFF and MALS has been reported [11] as a useful characterization tool for starch polymers. Also, flow FFF can be employed over a wide size range and does not suffer from any limitation regarding the fractionation of high-molecular-mass components. Consequently, together with MALS, flow FFF might be the method of choice for the size characterization of polysaccharides and other complex macromolecules. The aim of this study is therefore to determine if the hyphenated technique will be able to provide relevant information about molecular mass, radius of gyration and conformation for a number of pullulans and dextrans.

2. Theory

2.1. Asymmetrical flow field-flow fractionation

The separations in FFF take place in a thin, ribbon-like channel through which a liquid flow with a parabolic velocity profile is pumped. This flow will transport the sample axially along the channel. During the transport, the sample will also be exposed to a transverse force acting perpendicular to the direction of axial transport. When the transverse force is caused by a crossflow, the technique is called flow FFF. The separation principle in flow FFF is, in the normal mode (usually for particles below 0.5 μm in size) [1,12], strictly based on differences in diffusion coefficients, which makes the method capable of separating any components that differ in size and shape. Small sample components having large diffusion coefficients will get a higher elevation from the channel wall (the accumulation wall) and thus be transported faster through the channel due to the parabolic velocity profile of the transport flow (Fig. 1). Consequently, there will be a separation in time where the sample components are eluted in order of increasing size, which is in the opposite order to that of SEC.

Asymmetrical flow FFF is a variant of flow FFF, having one solid channel wall and one that is permeable to the flow [13]. The inlet flow in these channels is divided into a transverse crossflow, which exits through the permeable wall and an axial flow that transports the sample along the channel. The level of retention in asymmetrical flow FFF depends mainly on the ratio of the crossflow rate V_c and the outlet flow rate V_{out} [5]. At sufficiently high retention levels, the relation between the retention time, t_r, and the hydrodynamic diameter, d_H, is reduced to a simple linear relationship [5]

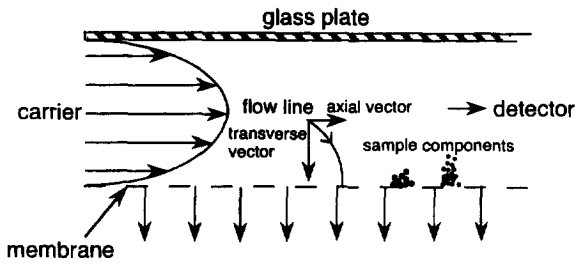

Fig. 1. The asymmetrical flow FFF channel. The carrier flow with a parabolic velocity profile is pumped along the channel. The sample components are influenced by the flow vectors that transport them in the axial direction to the detector (the axial vector) and press them towards the membrane (the transverse vector, crossflow). The separation in time is dependent on the sample position above the membrane, which, in turn, is determined by the diffusion coefficient of each component.

$$d_H = \frac{2kTA}{\pi\eta t^0 V_c w} t_r \quad (1)$$

where k is the Boltzmann constant, T is the temperature, A is the area of the porous membrane, η is the viscosity coefficient, t^0 is the void time and w is the channel thickness. For a more complete description of the theory of asymmetrical flow FFF the reader is referred to previous publications [5,10,13–15].

2.2. Multi-angle light scattering

Static light scattering is a well-known, absolute technique for measurements of molecular mass [16]. The molecular mass of a macromolecule from a light scattering experiment using low angles of measurement can be calculated by the relationship

$$\frac{Kc}{R_\theta} = \frac{1}{M} + 2A_2c \quad (2)$$

where the constant K is given by

$$K = \frac{4\pi^2 \bar{n}_0^2 (\partial n/\partial c)^2}{\lambda_0^4 N_A} \quad (3)$$

in which c is the solute concentration, R_θ is the excess Rayleigh factor, θ is the scattering angle, A_2 is the second virial coefficient, $\bar{n}_0$ is the refractive index of the solvent, $\partial n/\partial c$ is the refractive index increment of the polymer in solution, λ_0 is the wavelength of the light and N_A is Avogadro's number.

For a polydisperse sample, Eq. (2) can be written as

$$R_\theta = K\sum c_i M_i \quad (4)$$

and combined with the expression for the weight-average molecular mass,

$$M_w = \frac{\sum c_i M_i}{\sum c_i} \quad (5)$$

the well-known light scattering equation

$$\frac{Kc}{R_\theta} = \frac{1}{M_w} + 2A_2c \quad (6)$$

is obtained.

Eq. (6) is valid for any type of scatterer if the radial axis of the particle is less than 5% of the wavelength. If the particle is larger, the scattering from different parts of the particle will exhibit a difference in phase. The phase difference will be dependent on the scattering angle and increases as the observation angle is increased (the difference is 0 at $\theta = 0$). To compensate Eq. (6) for the decrease in scattering intensity, a special form factor $P(\theta)$ is introduced [17]

$$P(\theta) = 1 + \frac{16\pi^2\langle r_G^2\rangle}{3\lambda_0^2} \sin^2\left(\frac{\theta}{2}\right) \quad (7)$$

where $\langle r_G^2\rangle^{1/2}$ is the root mean square radius of gyration.

The form factor changes Eq. (6) into

$$\frac{Kc}{R_\theta} = \left[\frac{1}{P(\theta)}\right]\left[\frac{1}{M_w} + 2A_2c\right] \quad (8)$$

By measuring the scattering intensity at different angles and concentrations, a multi-angle light scattering instrument can provide information not only about molecular mass but also about the radius of gyration and the second virial coefficient.

2.3. Asymmetrical flow FFF–MALS

If the MALS instrument is connected to a separation system such as SEC or FFF with a concentration-sensitive detector, refractive index or

photometric, even more information can be obtained [16]. It is now possible to measure the scattering intensity in each small slice, i, of the fractionated sample

$$\frac{Kc_i}{R_{\theta_i}} = \left[\frac{1}{P(\theta)_i}\right]\left[\frac{1}{M_i} + 2A_2c\right] \quad (9)$$

and thus provide a molecular mass distribution, radius of gyration distribution and different averages of the molecular mass. The weight-average molecular mass and the number-average molecular mass, M_n, gives the polydispersity index, M_w/M_n. Since the concentration in each slice is not multiple, information about A_2 is not available. The A_2 term is however assumed to be negligible, due to the very low concentration in each slice [16]. Together with flow FFF, it is possible to obtain information about the hydrodynamic size of the macromolecule, which makes the combination of these two methods a powerful team in the characterization of polymers.

3. Experimental

3.1. Materials

The carriers were either pure, filtered water or filtered 0.1 M sodium chloride, both containing 0.02% sodium azide. The filter was a 0.2-μm regenerated cellulose filter SM 116 (Sartorius, Göttingen, Germany). The temperature in the carrier was around 297 K. Six pullulan standards (Shodex Standard P-82, Showa Denko, Tokyo, Japan) and three dextrans (Pharmacia, Uppsala, Sweden) were studied. They are listed in Table 1. The dry material was dissolved in the carrier medium and the solution was then filtered using an Anotop 25 Plus syringe filter, 0.1 μm pore size (Whatman International, Maidstone, UK). The total sample concentration was 5 mg/ml, if nothing else was stated, which corresponds to an injected amount of 100 μg. For the samples with low molecular mass (23 700–100 000 g mol^{-1}), higher sample concentrations of 10 and 15 mg/ml were used as well, in an attempt to increase the light scattering detector signal.

3.2. Methods

The FFF–MALS set-up is shown in Fig. 2. The FFF part is an ordinary asymmetrical flow FFF instrument that has been described previously [5,10,15]. The separation channel had a trapezoidal geometry defined by a Mylar (polymethylmetacrylate) spacer. The channel length, L, was 28.6 cm, the breadths, b_0 and b_L, were 2.1 and 0.54 cm,

Table 1
Weight-average molecular mass, M_w, and the polydispersity index, M_w/M_n obtained from FFF–MALS in the two carriers

Sample	Given data		Water			0.1 M NaCl		
	M_w	M_w/M_n	Recovery (%)	M_w	M_w/M_n	Recovery (%)	M_w	M_w/M_n
Dextran T70	66 300	1.82	83	78 800	1.8	88	79 200	2.2
Dextran T500	539 000	2.7	91	455 000	1.8	92	408 800	2.2
Dextran T2000			90	2 350 000	20	83	2 540 000	19
Dextran T2000 1[a]				288 200	4.6		358 700	3.3
Dextran T2000 2[a]				4 909 000	1.3		5 320 000	1.13
Pullulan P-20	23 700	1.07	93	24 600	1.07	86	26 600	1.04
Pullulan P-50	48 000	1.09	84	45 000	1.11	83	45 300	1.11
Pullulan P-100	100 000	1.10	94	92 400	1.07	89	97 700	1.14
Pullulan P-200	186 000	1.13	88	193 400	1.10	91	179 900	1.11
Pullulan P-400	380 000	1.12	85	403 800	1.10	93	401 100	1.07
Pullulan P-1600	1 660 000	1.19	91	1 426 000	1.04	90	1 374 000	1.03

The weight-average molecular mass, M_w, and the polydispersity index, M_w/M_n obtained from FFF–MALS in the two carriers are in good agreement with the given data from the manufacturer.
The recovery, obtained from the refractometer, of each sample injected is well above 80%.
[a] For dextran T2000, values of M_w and M_w/M_n are shown for the whole sample as well as for the low- (1) and the high- (2) molecular-mass components separately.

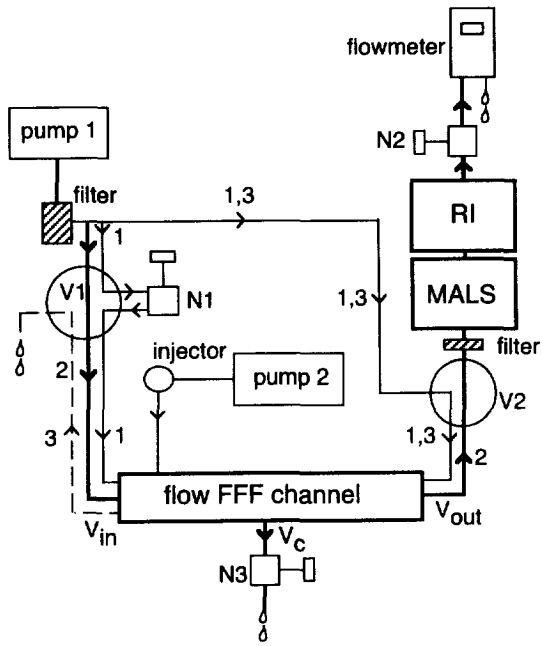

Fig. 2. The combined asymmetrical flow FFF–MALS system. The refractive index detector was connected directly after MALS. The flow from pump 1, which passed through an in-line filter, was directed by the valves V1 and V2 according to the three different experimental phases in each fractionation. The first step was the injection and the relaxation–focusing of the sample (1, thin lines). The position of the focusing point was regulated by needle valve N1. The second step was the elution (2, heavy lines), the sample was fractionated and the sample components were detected by the two detectors. For low-molecular-mass samples, an in-line filter between the channel and MALS was employed. The third step was a short backflushing of carrier liquid through the channel (3, thin lines). The crossflow rate versus the outlet flow-rate was directed by needle valves, N2 and N3 and the outlet flow-rate was measured by a flow meter.

respectively. The area of the accumulation wall was 33.65 cm^2. The channel thickness was calibrated with ferritin [14] to 0.0120 cm, giving a channel volume of 0.404 cm^3. The void time was calculated using the known data on the channel geometry and the flow-rates [5,15]. The ultrafiltration membrane was made of regenerated cellulose, NADIR UF 10c, cut-off 10 000 g mol^{-1} (according to the manufacturer, 80–90% of Dextran T10 is retained) (Hoechst, Wiesbaden, Germany). Two liquid chromatography pumps (Kontron HPLC-pump 420; Kontron Instruments, Zurich, Switzerland) delivered the carrier flow (pump 1) and the injection flow (pump 2), respectively. The flow from pump 1 was directed by two motor-driven valves, denoted V1 and V2 in Fig. 2. V1 was a Valco E-CST 4UV multi-position valve and V2 was a Valco E C4W 2 position valve (Vici, Valco Europe, Schenkon, Switzerland). The sample was injected using a Rheodyne 9125 syringe injector (Rheodyne, Cotati, CA, USA) with a 20-μl sample loop. The outlet flow-rate was continuously monitored by a PhaseSep liquid flow meter (Phase Separations, Queensferry, UK). Two fine metering needle valves (Hoke Valve 1656 G2YA, Hoke, Cresskill, NJ, USA) were used, one regulated the flow directions at relaxation/focusing and the other regulated the cross flow. The flow-rates delivered by pump 1 and the motor-valves V1 and V2 were directed by a Kontron Data System 450-MT2 (Kontron Instruments). The reader is referred to previous publications for details of the operational procedure of the asymmetrical flow FFF system [5]. A stainless steel filter-holder (Millipore, Bedford, MA, USA) with a 25 mm 0.1 μm filter (Anodisc 25, Anotec Separations, Banbury, UK) was connected on-line directly after pump 1. A small volume precolumn filter (A315; Upchurch Scientific, Oakharbor, WA, USA) with a replacable stainless steel frit (A102x; pore size 0.5 μm) surrounded by PTFE (the diameter of the stainless steel frit was 2.25 mm and the thickness was 1.55 mm) was employed in-line between the channel and the detector, when needed. Filtering was performed by inserting a piece of 0.45-μm regenerated cellulose filter (SM 116), cut to a suitable size, on top of the stainless steel frit.

The light scattering photometer was a DAWN-DSP MALS system (Wyatt Technology, Santa Barbara, CA, USA). Concentration detection was performed with an Optilab DSP interferometric refractometer (Wyatt Technology). Both detectors were used at a wavelength of 633 nm. Filtered toluene (Merck, Darmstadt, Germany) was used for the calibration of the MALS detector and sodium chloride (Suprapur, Merck, Darmstadt, Germany) was used for the calibration of the refractive index (RI) detector. The MALS instrument was normalized using pullulan P-50 and bovine serum albumin. The signals from the two detectors were analyzed by the ASTRA software (Wyatt Technology). The RI increment, $\partial n/\partial c$, was experimentally determined for both pullulan and dextran from different concentration

series of each polysaccharide injected into the refractometer. Then the $\partial n/\partial c$ value was obtained using the DNDC software (Wyatt Technology). For pullulan, $\partial n/\partial c$ values of 0.137 (in water) and 0.138 (in 0.1 *M* NaCl) were obtained, whereas for dextran, the corresponding values were 0.142 and 0.137, respectively. The recovery was obtained from the ratio of the mass eluted from the channel (determined by integration of the refractometer signal) and the injected mass.

4. Results and discussion

Dextrans and pullulans are industrially important polysaccharides [18–21]. Dextran is produced by microorganisms (*Leuconostoc dextrans*) and is, for example, known to be a blood plasma-volume expander. It is an anhydroglucan, consisting mainly of 1-6-glucosidic linkages. Pullulan is produced by the yeast-like fungus *Aureobasidium pullulans*. It consist of 1-6-linked maltotriose units and has a more linear structure than dextran [18]. Pullulan and dextran are commonly used as molecular mass standards in, for example, SEC. Information about the molecular mass distribution is crucial for this application and is often obtained using SEC or ultracentrifugation. In this work, we have chosen a range of pullulan and dextran standards as model compounds for polysaccharides, and other water-soluble polymers, to study the ability of the instrumental combination of asymmetrical flow FFF–MALS to characterise molecular mass, molecular size and conformation. The potential advantages of flow FFF are that (1) it can separate polymers over a very wide molecular mass range using a change of flow-rates as the only means of adjusting the conditions to fit a certain molecular mass range; (2) it is applicable to large molecules stretching far into the multimillion molecular mass range; (3) it involves short separation times (below 10 min), no matter what molecular mass the sample covers, which can easily be obtained by adjusting the flow-rates; and (4) diffusion coefficients and hydrodynamic diameters can be determined without calibration. The six pullulans chosen represent a wide range of molecular masses from 20 000 to 1 600 000 g mol^{-1}, all having a low polydispersity. The three dextrans, on the other hand, had a high or partly unknown polydispersity and also covered a broad molecular mass range from 70 000 to 2 000 000 g mol^{-1}. In the results described below, care was taken to adjust the flow-rates in each case so that the analysis time was always short, in the range of 5 min or lower. Experiments were done using carriers made up of either pure water or 0.1 *M* sodium chloride. This served to detect if the ionic strength could influence the results, for example, if the ultrafiltration membrane or the polysaccharides contained any carboxylic acid residues [3].

4.1. Molecular mass

The lower limit in molecular mass using flow FFF is determined by the cut-off of the ultrafilter, in this case 10 000 g mol^{-1}. This corresponds to a hydrodynamic diameter cut-off in the range of a few nm for many macromolecules. This means that a certain fraction of a polydisperse sample may be lost through the ultrafilter so that the observed average molecular mass may be overestimated. Another limitation is the weak retention that is often obtained (depending on the limitations in the crossflow) for molecular sizes corresponding to a few nm hydrodynamic diameter. Weak retention gives low resolution [5,22] in flow FFF and thus attempts to measure the size distribution may be meaningless. A third limitation may occur for relatively small macromolecules where the light scattering signal is weak and therefore easily disturbed by noise.

The first attempts to characterize the low-molecular-mass pullulans and dextrans (Dextran T70, Pullulan P-20, P-50 and P-100) were problematic. The light scattering signals were weak and noisy, which resulted in low precision in the calculated molecular mass. An increase in the injected amount of the sample improved the responses slightly, but resulted also in channel overloading effects, which were observed as decreased retention times. Furthermore, a bimodal peak shape was seen with MALS, both for pullulans and dextrans, but was not detected by the refractometer (Fig. 3). This resulted in erroneous and irreproducible molecular mass distributions, as seen for two different runs of Dextran T70 in Fig. 4 (curves b and c) and appeared in either of the two carrier liquids. Introducing a small-volume 0.45-μm in-line filter between the channel outlet and the

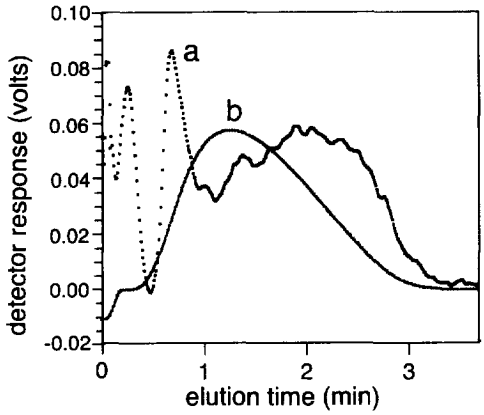

Fig. 3. The responses obtained, without the in-line filter between the channel and detectors, from the MALS detector (a; 90° signal) and the refractive index detector (b) shown for dextran T70. Carrier: water. Conditions: $V_{in}=4.0$ ml/min; $V_{out}=0.88$ ml/min; $V_c/V_{out}=3.5$; $t^0=0.19$ min.

MALS detector increased the signal-to-noise ratio dramatically. Moreover, the 0.75-min peak observed in Fig. 3 disappeared so that the MALS response curve became monomodal, which was more reasonable in comparison to the RI signal. The molecular mass distribution consequently became much more reasonable (curve a in Fig. 4) and the results were reproducible. The presence of the 0.75-min extra peak may be explained by dust or aggregates in the injected sample having a much larger molecular mass than Dextran T70 but having a smaller hydrodynamic size. Another possibility is that there were μm-sized particles that travelled through the channel in the hyperlayer mode [12]. The extra peak was much less pronounced relative to the main peak when the higher molecular mass samples were analysed.

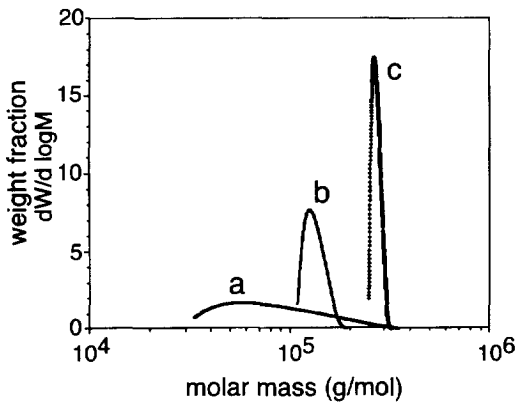

Fig. 4. The molecular mass distribution of dextran T70 with (run a) and without (runs b and c) the in-line filter. Carrier: water. Conditions (a–c): $V_{in}=4.0$ ml/min; $V_{out}=0.88$ ml/min; $V_c/V_{out}=3.5$; $t^0=0.19$ min.

After replacing the ultrafiltration membrane with a fresh one, the extra peak disappeared. This was so even if the in-line filter was not used, which indicates that the appearance of the extra peak was related to pollution of the membrane surface. The use of the in-line filter was still necessary, however, because it greatly improved the signal-to-noise ratio for the low-molecular-mass pullulans and dextrans, which made it possible to obtain good precision in the molecular mass estimations and these reliable results are presented in Table 1. The recovery of the injected mass was well above 80% for all samples analysed, which indicates that no major losses of the injected sample occurred. In addition, the recovery was not influenced by the in-line filter, as this had a relatively large pore size. The low-molecular-mass pullulan standards showed a low polydispersity index, in the range between 1.04 and 1.14, which is in excellent agreement with the data given by the manufacturer. The obtained molecular mass averages are also in good agreement with the given data, showing a maximal deviation of only 12%. Dextran T70 has, as expected, a broader molecular mass distribution and the polydispersity index was around two. In Fig. 5, the molecular mass distributions for dextran T70 and pullulan P-100 are shown. Apparently, a large amount of the dextran sample has a molecular mass of below 70 000 g mol^{-1}, however, a high-molecular-mass tail with a molecular mass of up to 300 000 g mol^{-1} increased the weight-average molecular mass to 79 000 g mol^{-1}. The given weight-average molecular mass from the manufacturer was rather similar, 66 300 g mol^{-1}, which is a good agreement, taking into account the very wide size distribution of this sample. For the pullulan P-100, a narrow molecular mass distribution that was centered around 100 000 g mol^{-1} was obtained (Fig. 5) and the achieved weight average was in good agreement with that given by the manufacturer (Table 1). The results are similar in water and in sodium chloride.

In analysing the high-molecular-mass samples

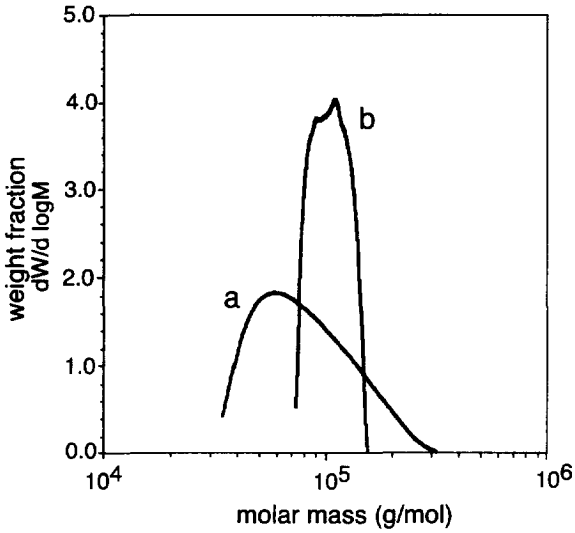

Fig. 5. The molecular mass distribution of dextran T70 (a) and pullulan P-100 (b). Carrier: water. Conditions: (a) $V_{in}=4.0$ ml/min; $V_{out}=0.88$ ml/min; $V_c/V_{out}=3.5$; $t^0=0.19$ min; (b) $V_{in}=4.0$ ml/min; $V_{out}=1.01$ ml/min; $V_c/V_{out}=3.0$; $t^0=0.18$ min.

(dextran T500 and T2000; pullulan P-200 to P-1600) all experiments were done without using the in-line filter between the channel and the detectors. It was no longer needed because the much higher light scattering signals from the large molecules gave signal-to-noise ratios that were high enough to obtain good precision in the measurements. The molecular mass averages and polydispersity indices obtained are shown in Table 1. The pullulans (P-200 to P-1600) showed a low polydispersity, in good agreement with the manufacturer's data, which was also true for the averages. However, pullulan P-1600 gave, in our measurements, smaller values for the polydispersity, the latter being lower than for most of the other pullulans. Furthermore, the M_w turned out to be around $1.4\cdot10^6$, which is somewhat lower than the value given by the manufacturer. If the M_w was thus really underestimated, it may have lead to lower polydispersity values than expected. This seems less likely, however, since the obtained data for the other pullulans are in good agreement with the given values and the same instrumental calibration constants were used. All pullulans, except P-1600, gave molecular mass averages that coincided with those of the manufacturer to within 2–12%.

In Fig. 6, fractograms of dextran T500 registered

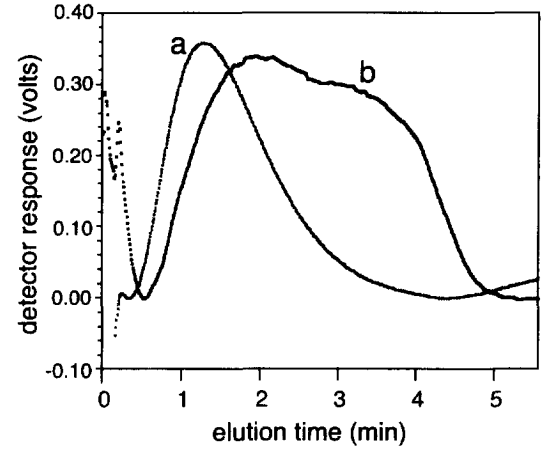

Fig. 6. The responses from the RI detector (a) and the MALS detector (b; 90° signal) for dextran T500. Carrier: 0.1 *M* NaCl. Conditions: $V_{in}=2.0$ ml/min; $V_{out}=0.89$ ml/min; $V_c/V_{out}=1.2$; $t^0=0.27$ min.

by the RI detector and the light scattering detector at 90° are shown. The light scattering signal was much higher than the RI signal in the latter part of the response curve, which is typical for a significantly polydisperse sample. This is explained by the fact that the light scattering detector is more sensitive for the large-sized sample components, which are eluted last in FFF. Fig. 7 shows the molecular mass versus elution time for dextran T500 and pullulan P-1600. For both samples, the molecular mass increases with the elution time, as expected and in agreement with FFF theory.

Pullulan P-1600 is, as mentioned, a sample with low polydispersity and the variation of the molecular mass with time is consequently small. The increase in the molecular mass at the end of the pullulan peak could probably be explained by the different nature of the responses from the MALS and RI detectors, respectively. The response from the refractometer only reflects changes in concentration, whereas the light scattering detector is influenced both by the molecular mass and by the concentration of the sample. At the end of the peak, high molecular mass macromolecules of low concentration are present, which may lead to a very uncertain, almost zero, concentration signal being determined by the refractometer. This makes the calculation of molecular mass unreliable.

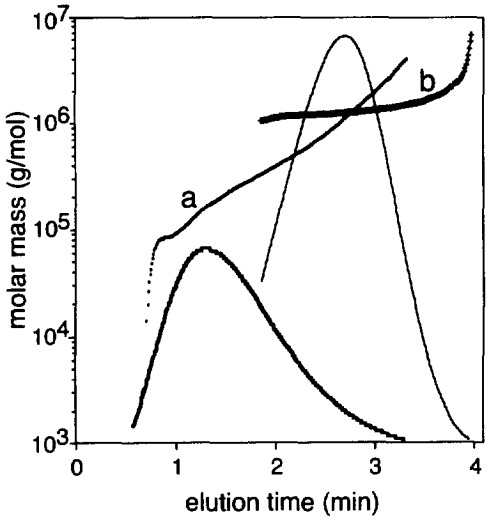

Fig. 7. The molecular mass versus the elution time for dextran T500 (a) and pullulan P-1600 (b). The refractive index fractograms of each sample are superimposed. Carrier: 0.1 *M* NaCl. Conditions: (a) $V_{in}=2.0$ ml/min; $V_{out}=0.89$ ml/min; $V_c/V_{out}=1.2$; $t^0=0.27$ min; (b) $V_{in}=1.75$ ml/min; $V_{out}=1.24$ ml/min; $V_c/V_{out}=0.41$; $t^0=0.25$ min.

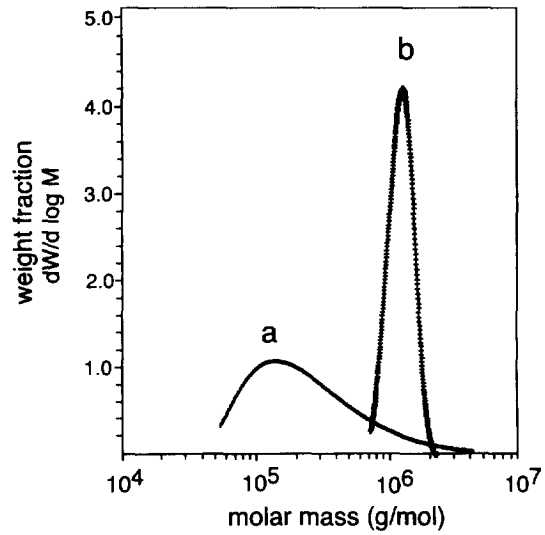

Fig. 8. The molecular mass distribution of dextran T500 (a) and pullulan P-1600 (b). Carrier: 0.1 *M* NaCl. Conditions: (a) $V_{in}=2.0$ ml/min; $V_{out}=0.89$ ml/min; $V_c/V_{out}=1.2$; $t^0=0.27$ min; (b) $V_{in}=1.75$ ml/min; $V_{out}=1.24$ ml/min; $V_c/V_{out}=0.41$; $t^0=0.25$ min.

The narrow molecular mass distribution of pullulan P-1600 is illustrated in Fig. 8. Such narrow distributions would have been difficult to measure without the MALS detector, e.g. directly from the concentration vs. elution time curves using some relationship between the diffusion coefficients and molecular mass [3]. The difficulty lies in the need to quantitate the contribution of instrumental band broadening to the observed band width. Without such compensation, the result would be an over-estimation of the polydispersity of pullulan P-1600. The combination of flow FFF with the light scattering detector avoids this difficulty and more reliable molecular mass distributions can be achieved.

Dextran T500 gave a much higher increase in the molecular mass with time than did pullulan P-1600, as seen in Fig. 7. Consequently, the T500 molecular mass distribution is broad, with a polydispersity index of around two. Similar to dextran T70, there is a high-molecular-mass tail, in this case including masses of up to $3\cdot10^6$ g mol^{-1}.

For the dextran T2000, unlike the other dextrans, there was no information available from the manufacturer about the molecular mass averages or distributions. Our results are shown in Fig. 9, where the superimposed light scattering and RI signals are given. The refractometer detected a curve with a significant bimodal shape and populations centering

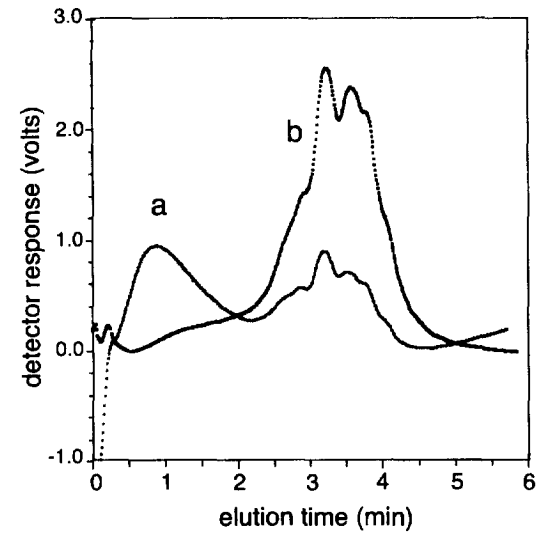

Fig. 9. The responses from the refractive index detector (a) and the MALS detector (b; 90° signal) for dextran T2000. Carrier: 0.1 *M* NaCl. Conditions: $V_{in}=2.0$ ml/min; $V_{out}=1.04$ ml/min; $V_c/V_{out}=1.0$; $t^0=0.26$ min.

around 1 and 3.5 min, respectively, whereas the 90° light scattering signal showed only one evident population (from 2.5 to 4.5 min), but a slight tendency to a population at around 1.5 min. This indicates that dextran T2000 consists of one low- and one high-molecular-mass component. Dextran T2000 thus turned out to have a more complex composition than dextran T500. The weight-average molecular mass for the whole sample is slightly above $2 \cdot 10^6$ g mol^{-1} (Table 1), which is in agreement with the expectations based on the product information from the manufacturer. The polydispersity index is very high, around twenty, reflecting the bimodal distribution of the sample. When the low (0.5–2 min)- and high (2–4.5 min)-molecular-mass components were analysed separately using ASTRA software, the low-molecular-mass components had a weight-average molecular mass of around 300 000 g mol^{-1} and a polydispersity of four. The corresponding parameters for the high-molecular-mass component were $5 \cdot 10^6$ g mol^{-1} and 1.2. The molecular mass distribution for dextran T2000, showing the presence of the two size populations, is illustrated in Fig. 10. The two experiments illustrated were obtained using water and 0.1 *M* sodium chloride as carriers, respectively, and shows no significant difference. The noise appearing in the distribution curves in the molecular mass range above $2 \cdot 10^6$ is caused by the noise in each of the detector signals (see Fig. 9). This noise is

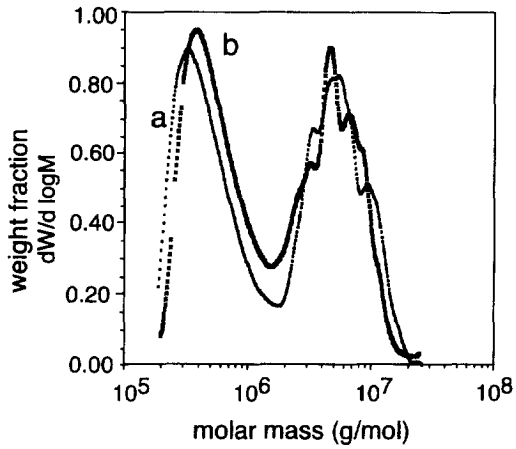

Fig. 10. The molecular mass distribution of dextran T2000 in water (a) and in 0.1 *M* NaCl (b). Conditions: $V_{in} = 2.0$ ml/min; $V_{out} = 1.04$ ml/min; $V_c/V_{out} = 1$; $t^0 = 0.26$ min.

difficult to explain and our experience indicates that it often occurs when polymers in the multimillion molecular mass range are fractionated.

4.2. Molecular size

From the diffusion coefficient, it is possible to calculate the hydrodynamic diameter, d_H, according to the Stokes–Einstein equation (Eq. (1)). This parameter will give the equivalent sphere diameter of a macromolecule in solution, which may be difficult to interpret if the conformation is unknown. However, if the molecular mass is known, the combination of these with the hydrodynamic diameters (or diffusion coefficients) gives some information on the shape of the polymer. Thus, the hydrodynamic diameters measured from the observed elution time in FFF provide useful information if the molecular mass has been determined from MALS in the same experiment.

The root mean square radius of gyration, $\langle r_G^2 \rangle^{1/2}$, can be obtained with MALS as well (described by Eqs. (7,9)) [16]. The $\langle r_G^2 \rangle^{1/2}$ determination does not require any data for $\partial n/\partial c$, molecular mass or concentration and is thus insensitive to any errors in these, therefore, in cases where these parameters are difficult to obtain, one can at least determine the $\langle r_G^2 \rangle^{1/2}$ [16]. One limitation in using MALS is that $\langle r_G^2 \rangle^{1/2}$ values below 10 nm are not obtained, which may be a disadvantage when working with small macromolecules.

Fig. 11A shows an example of a fractionation where the retention times have been transformed into hydrodynamic diameters. This followed known procedures [5]. The sample was pullulan P-1600. The fractograms from all other pullulan samples and all dextran samples were treated similarly and the hydrodynamic diameters read at the peak maxima are reported in Table 2. The two fractograms shown in Fig. 11A are exceptional in that they gave, for the same sample, different ranges of hydrodynamic diameters. This is a deviation that sometimes occurs with polymers having large hydrodynamic diameters that are being analysed at high crossflow rates. An additional problem was that the responses were very noisy, making it difficult to locate the peak maxima. When the crossflow was reduced, to give lower

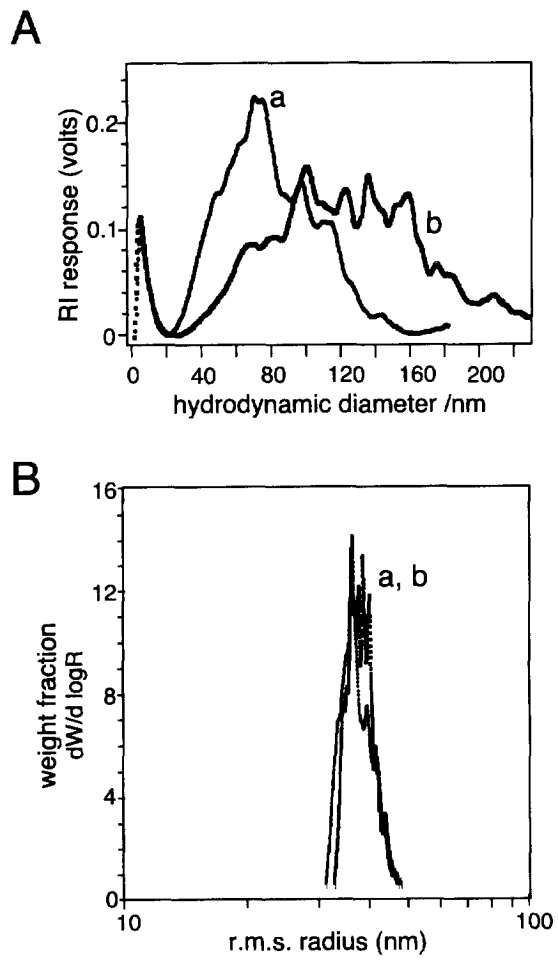

Fig. 11. (A) Two refactive index fractograms of pullulan P-1600 obtained at different flow-rates. Carrier: 0.1 *M* NaCl. Conditions: (a) $V_{in}=1.75$ ml/min; $V_{out}=1.03$ ml/min; $V_c/V_{out}=0.70$; $t^0=0.27$ min and (b) $V_{in}=2.0$ ml/min; $V_{out}=0.97$ ml/min; $V_c/V_{out}=1.1$; $t^0=0.26$ min. (B) The corresponding root mean square radius distribution for (a) and (b).

degrees of retention [5], the hydrodynamic diameters became consistent and noise-free. Such conditions were chosen for all data presented in Table 2 and are illustrated by the fractogram of pullulan P-1600 in Fig. 7, which demonstrates the smooth noise-free curve obtained under the milder flow conditions. The peak maximum hydrodynamic diameters obtained were from around 10 nm for pullulan P-20 up to over 70 nm for pullulan P-1600, and from 10 nm for dextran T70 to 60 nm for the high-molecular-mass component of dextran T2000.

The *z*-average root mean square radii obtained for the pullulans and the dextrans using MALS are summarised in Table 2. In analysing the data from the pullulan P-1600, obtained under the flow conditions mentioned above that gave inconsistent hydrodynamic diameters, it was found that the $\langle r_G^2\rangle^{1/2}$ distributions were identical for the two runs (see Fig. 11B). This would be expected because the calculation of $\langle r_G^2\rangle^{1/2}$ is performed independently and only requires that the polymer is subjected to size fractionation in the channel.

No values were obtained for the low-molecular-mass pullulans and dextrans, as expected, because their sizes were below 10 nm. This limitation of MALS is also illustrated by the fractionation of dextran T500 in Fig. 12, where $\langle r_G^2\rangle^{1/2}$ is plotted versus the elution time. Here, the values below 10 nm appear to be incorrect, as they change too rapidly. Another observation is that the $\langle r_G^2\rangle^{1/2}$ plot tends to flatten out at longer elution times although the molecular mass increases, as seen in Fig. 7.

The value of $\langle r_G^2\rangle^{1/2}$ increased from 11 nm for pullulan P-100 up to almost 40 nm for pullulan P-1600. The obtained data for pullulan P-100 may be unreliable, because they are close to the lower size limit for the determination of $\langle r_G^2\rangle^{1/2}$. For the same reason, data were only obtained for the high-molecular-mass fractions of dextran T500 and dextran T2000. Neither the hydrodynamic diameter nor the radius of gyration were greatly influenced by the carrier chosen, which indicates that the ionic strength had no influence on the obtained results.

4.3. Conformation

Knowledge of the conformation of a macromolecule in solution is of fundamental importance. The usual way of obtaining this information is to connect the intrinsic viscosity, $[\eta]$, with the molecular mass [23]

$$[\eta]=C_1M^{\alpha} \tag{10}$$

which is the so-called Mark–Houwink equation. Similar relationships have been established also between the radius of gyration and the molecular mass

$$\langle r_G^2\rangle^{1/2}=C_2M^{\beta} \tag{11}$$

Table 2
Hydrodynamic diameter, d_H, calculated for the peak maxima (RI signal) and the z-average root mean square radii of gyration $\langle r_G^2 \rangle_z^{1/2}$ listed for the pullulans and the dextrans

Sample	Water		0.1 *M* NaCl	
	d_H (nm)	$\langle r_G^2 \rangle_z^{1/2}$ (nm)	d_H (nm)	$\langle r_G^2 \rangle_z^{1/2}$ (nm)
Dextran T70	12		8	
Dextran T500	22	17	17	16
Dextran T2000 1[a]	14		16	
Dextran T2000 2[a]	53	27	60	34
Pullulan P-20	9		10	
Pullulan P-50	15		14	
Pullulan P-100	24	12	20	11
Pullulan P-200	26	23	31	24
Pullulan P-400	57	29	51	27
Pullulan P-1600	76	37	72	39

[a] For dextran T2000, separate values are given for the low- (1) and the high- (2) molecular-mass components, respectively.

and between the diffusion coefficient, D, and molecular mass

$$D = C_3 M^{-\gamma} \quad (12)$$

The exponents α, β and γ give information about the conformation of the macromolecule [23] and C_1, C_2 and C_3 are constants. With a flow FFF–MALS system, it is possible to the obtain the diffusion coefficient, the radius of gyration and the molecular mass. Thus, exponents β and γ, respectively, can be determined using Eqs. (11,12). Such data are summarised in Fig. 13. The logarithmic plot of $\langle r_G^2 \rangle^{1/2}$ versus molecular mass, in Fig. 13A, illustrates the determination of the exponent β for pullulan P-400 and P-1600 and for dextran T500 and T2000 using the salt carrier. The slope, β, is 0.59 for both pullulans, which represents a random coil conformation. The dextrans show more complex conformational behaviour. The slope for dextran T500 showed a tendency to decrease with increasing molecular mass and the average behaviour, expressed by the slope, 0.36, of all data points, therefore indicates a more compact conformation of the dextrans than of the pullulans. The decreasing slope suggests that the high molecular end of the distribution consists of more branched, compact macromolecules. The plot of dextran T2000, using only the high-molecular-mass components, gave an exponent of 0.27, which suggests a highly branched structure.

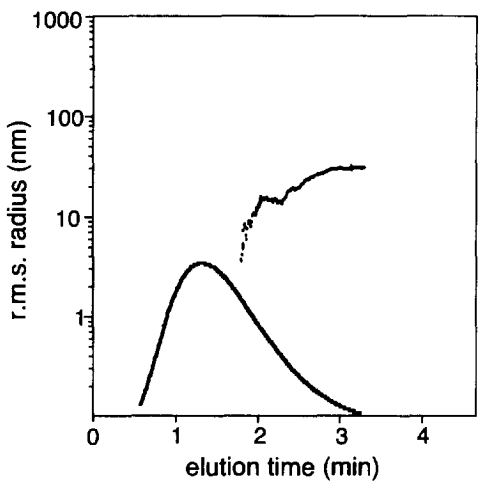

Fig. 12. The root mean square radius of gyration versus the elution time for dextran T500. The refractive index fractogram is superimposed. Carrier: 0.1 *M* NaCl. Conditions: $V_{in} = 2.0$ ml/min; $V_{out} = 0.89$ ml/min; $V_c/Vout = 1.2$; $t^0 = 0.27$ min.

The use of Eq. (12) is illustrated in Fig. 13B by a logarithmic plot of the diffusion coefficients against molecular mass for all dextran and pullulan samples. Each diffusion coefficient, D_i, and the corresponding molecular mass, M_i, were obtained at the peak maximum of each RI response curve for each sample. Similar to the β exponents (Fig. 13A), the γ exponent for the pullulans, 0.58, indicates a random coil conformation. The slope (0.38) of the dextran plot supports the previous findings from the radius of gyration plot that the dextrans have a more compact structure than the pullulans. It is noteworthy that the three lowest-molecular-mass dextrans tend to fall on a line having a lower slope value than that of the

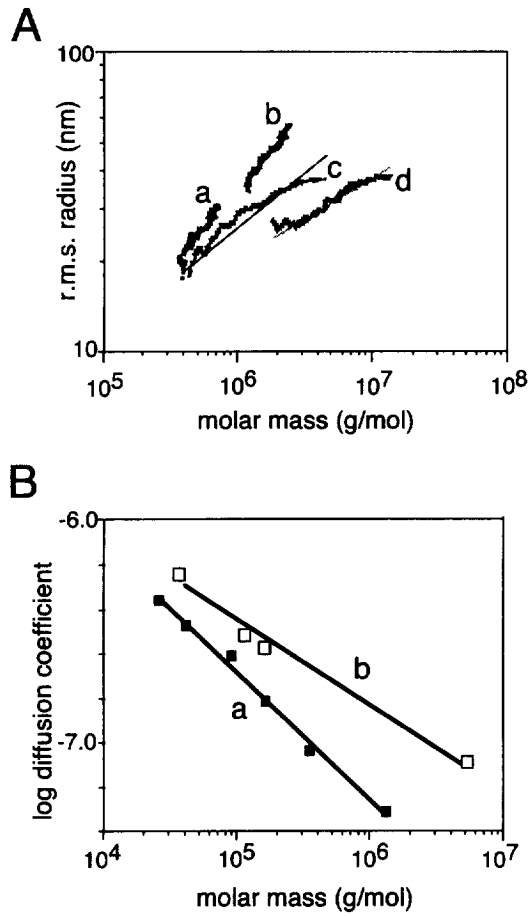

Fig. 13. (A) Plot of the root mean square radius of gyration versus the molecular mass for pullulan P-400 (a), pullulan P-1600 (b), dextran T500 (c) and dextran T2000 (d). Carrier: 0.1 *M* NaCl. The slope, β, was 0.59 for (a), 0.58 for (b), 0.36 for (c) and 0.27 for (d). (B) Plot of the log diffusion coefficient versus the molecular mass for the six pullulans (a) and the three dextrans (b). Dextran T2000 is represented by two points corresponding to the low- and high-molecular-mass components, respectively. Carrier: 0.1 *M* NaCl. The slope, γ, was 0.58 for (a) and 0.38 for (b).

regression line for all four dextrans, which means that they may have a less compact conformation than the high-molecular-mass components of dextran T2000. This indicates an increased branching at higher molecular masses, as already noted from the radius of gyration data above.

Our data on conformation expressed by the β exponent coincide very well with a recent similar study [24] on pullulans using SEC–MALS, resulting in $\beta = 0.56$. It is also well known from the literature that pullulans are regarded as rather flexible coils [18,19]. Also for the dextrans, our result is similar to that of a dextran sample studied by SEC–MALS with $\beta = 0.38$ [24]. However, in a similar study to ours, also using flow FFF–MALS [7], a dextran sample was found to have $\beta = 0.50$. In the literature, reported values for dextran range between 0.40–0.60 [7] and such variation may be possible depending on the variation in the origin and molecular mass range of the dextran studied.

Acknowledgments

This study was supported by grants from the Swedish Research Council for Engineering Sciences. The development of the flow FFF system was made possible by grants from Astra Hässle AB, the Carl Trygger Foundation and the Crafoord Foundation. M. Sc. Gunilla Nilsson is gratefully acknowledged for the generous gift of the dextran samples.

References

[1] J.C. Giddings, Science, 260 (1993) 1456.
[2] J.C. Giddings, Sep. Sci., 1 (1966) 123.
[3] J.J. Kirkland, C.H. Dilks and S.W. Rementer, Anal. Chem., 64 (1992) 1295.
[4] J.C. Giddings and M.A. Benincasa, Anal. Chem., 64 (1992) 790.
[5] B. Wittgren, K.-G. Wahlund, H. Derand and B. Wesslén, Macromolecules, 29 (1996) 268.
[6] B. Wittgren, K.-G. Wahlund, H. Derand and B. Wesslén, Langmuir, (1996), in press.
[7] D. Roessner and W.-M. Kulicke, J. Chromatogr. A, 687 (1994) 249.
[8] H. Thielking, D. Roessner and W.-M. Kulicke, Anal. Chem., 67 (1995) 3229.
[9] H. Thielking and W.-M. Kulicke, Anal. Chem., 68 (1996) 1169.
[10] A. Litzén, J.K. Walther, H. Krischollek and K.-G. Wahlund, Anal. Biochem., 212 (1993) 469.
[11] R. Hanselmann, M. Ehrat and H.M. Widmer, Starch, 46 (1995) 345.
[12] S.K. Ratanathanawongs and J.C. Giddings, Anal. Chem., 64 (1992) 6.
[13] K.-G. Wahlund and J.C. Giddings, Anal. Chem., 59 (1987) 1332.
[14] A. Litzén and K.-G. Wahlund, Anal. Chem., 63 (1991) 1001.
[15] A. Litzén, Anal. Chem., 65 (1993) 461.

[16] P.J. Wyatt, Anal. Chim. Acta, 272 (1993) 1.
[17] B.H. Zimm, J. Chem. Phys., 13 (1945) 141.
[18] J.F. Kennedy and C.A. White, in E. Haslam (Editor), Comprehensive Organic Chemistry, Vol. 5, Pergamon Press, Oxford, 1987, Ch. 26.3, p. 755.
[19] T. Kato, T. Okamoto, T. Tokuya and A. Takahashi, Biopolymers, 21 (1982) 1623.
[20] K. Gekko and H. Noguchi, Biopolymers, 10 (1971) 1513.
[21] C. Israelidis, B. Scanlon, A. Smith, S.E. Harding and K. Jumel, Carbohydr. Polym., 25 (1994) 203.
[22] J.C. Giddings, G.-C. Lin and M.N. Myers, J. Coll. Interf. Sci., 65 (1978) 67.
[23] E.G. Richards, An Introduction to Physical Properties of Large Molecules in Solution, Cambridge University Press, Cambridge, 1980.
[24] D. Nagy, J. Appl. Polym. Sci., 59 (1996) 1479.